Structural Chemistry (2024) 35:253–264
https://doi.org/10.1007/s11224-023-02178-0

RESEARCH

The second-order nonlinear optical properties of novel triazolo[3,4-b][1, 3, 4] thiadiazole derivative chromophores using DFT calculations

Balachandar Waddar[1] · Saidi Reddy Parne[1] · Suman Gandi[1] · Gurusiddappa R. Prasanth[2] · Mohammed Yaseen[3] · Mahadevappa Y. Kariduraganavar[3]

Received: 24 January 2023 / Accepted: 20 April 2023 / Published online: 10 May 2023

Abstract
Many organic chromophores possess excellent nonlinear optical (NLO) properties. In spite of this, the performance of these chromophores in second-order nonlinear optical applications is limited due to the high symmetry and short dipole moment of the parent molecules, which can lead to a weak response or high susceptibility to molecular orientation dependency. To address this challenge, we designed a series of new [1,2,4] triazolo[3,4-b] [1,3,4] thiadiazole derivative chromophores C1–C7 and studied their second-order NLO property through density functional theory (DFT) by substitution of different donor functional groups. To this end, several hybrid functionals such as B3LYP/6–311 + + G (d, p), CAM B3LYP/6–311 + + G (d, p), and ωB97XD/6–311 + + G (d, p) were employed to carry out quantum chemical calculations, which included calculations and evaluations of frequency-dependent dipole moment, linear polarizability, and first hyperpolarizability values. In addition, natural bond orbital (NBO) analysis, intramolecular charge transfer (ICT) mechanism, electronic charge density analysis, highest occupied molecular orbital (HOMO), lowest unoccupied molecular orbital (LUMO), and vertical energy transitions are studied with time-independent and time-dependent level density functional theory. The results demonstrate that C7 is the most efficient chromophore among the other chromophores investigated, with a significant first hyperpolarizability value of $105{,}032.98 \times 10^{-34}$. This study provides insights into how to design second-order NLO active organic chromophores with better performance for optoelectronic applications.

Keywords Nonlinear optical property (NLO) · Natural bond orbital (NBO) · [1, 2, 4] triazolo[3,4-b] [1, 3, 4] thiadiazole · Highest occupied molecular orbital (HOMO) · Lowest unoccupied molecular orbital (LUMO) · Density functional theory (DFT)

Introduction

Nonlinear optical (NLO) materials are active components of major modern photonic devices. They are used in a wide range of applications such as frequency generation, high processing of optical information, handling of high-density optical data storage devices, image processing techniques, bio-imaging, laser technology, and other highly NLO-influenced industrial applications ranging from 10^5 MHz to 10 THz [1–9]. The NLO response of an atom is the effect of the electric potential experienced by its electrons in NLO material systems [10, 11]. Second harmonic generation (SHG) is one of the most extensively studied phenomena in NLO materials and is employed for second-order NLO effects. In addition, second-order nonlinear optical materials have a broad range of applications in biology, material science, and medicine [12–14].

In recent years, numerous theoretical and experimental research groups have reported a significant number of second-order NLO materials [15–19]. In addition, the current trends in organic NLO materials have piqued the interest of numerous individuals due to their low cost, adaptability to other materials, high mechanical strength, and high photoelectric coefficients in comparison to other conventional materials such as inorganic and other complex material systems [20, 21]. In organic molecules, the NLO

✉ Saidi Reddy Parne
psreddy@nitgoa.ac.in

[1] Department of Applied Sciences, National Institute of Technology Goa, Farmagudi, Ponda, Goa 403401, India

[2] Department of Electronics & Communication Engineering, National Institute of Technology Goa, Farmagudi, Ponda, Goa 403401, India

[3] Department of P.G Studies in Chemistry, Karnatak University, Dharwad, Karnataka 580003, India

properties arise weak intramolecular bonding like van der Waals, dipole–dipole interactions, and hydrogen bonds. This interaction can cause the electrons to oscillate at very high frequencies, leading to a large change in the optical response of the molecule [22]. The nonlinear optics theory is a crucial and effective tool for understanding and developing novel organic NLO materials [23]. NLO responses of organic molecules can be several orders greater than those of inorganic molecules in response to an applied electric field [21, 24]. This large NLO response is due to the π-bond system, which entails the delocalized distribution of electric charges. In general, organic molecules that include conjugated π bonds are more polarizable than those that do not contain such bonds. This polarity results in an increased molecular response to an applied electric field. In addition, organic molecules are often less symmetrical than inorganic molecules, providing more molecular disorder that can contribute to increased NLO responses. However, designing materials with large NLO responses is difficult due to the limited conjugated chain length and the combination of efficient charge donors and acceptors of effective functional groups. The density functional theory (DFT) route allows for a better understanding of D-π-A interactions and can lead to the development of high hyperpolarizabilities of NLO active organic compounds [25, 26].

A limited number of second-order nonlinear optical (NLO) active and biologically active D-π-A system potential NLO organic compounds have been reported in the literature [27–32]. Recently, [1,2,4] triazolo[3,4-b] [1,3,4] thiadiazole, an azo class constituent unit of a few chemical systems, has become of particular interest in this system. It is believed that the majority of these molecules have a π-conjugated bridge, which plays a crucial role in the function of NLO. Even though these compounds have the potential to become NLO materials, additional research is required to evaluate whether or not this is indeed possible. For instance, a series of new 6-sulfonyl-1,2,4-triazolo[3,4-b][1,3,4]thiadiazole derivatives are being investigated experimentally for the antibacterial activity for photosynthesis-related proteins applications [27]. Radwan et al. studied the biological characteristics of 1,3,4-thiadiazole- and 1,2,4-triazole-3(4H)-thione-containing salicylate compounds for antifungal applications [28]. Additionally, 3,6-disubstituted-1,2,4-triazolo-1,3,4-thiadiazole and 3,6-distributed 1,2,4-traizolo [3,4-b]1,3,4-thiadiazole compound derivatives are showed excellent antimicrobial activities [29, 30]. The results of experimental research on 4-amino-5-mercapto-1,2,4-triazoles suggest that these compounds are appropriate for use in anticancer applications [33]. Similarly, the results of an experimental study on the s-triazolo[3,4-b]-thiadiazole heterocycle demonstrate a high degree of optical nonlinearity for organic chromophores [34], suggesting that these NLO active compounds are present. [1,2,4] triazolo[3,4-b] [1,3,4] thiadiazole heterocyclic ring as a molecule's acceptor exhibits excellent first hyperpolarizability, and this donor and acceptor group combination increases mechanical and thermal stability via polymeric crosslinking methods that are highly NLO active [35, 36].

Previous studies demonstrated that [1,2,4] triazolo[3,4-b] [1,3,4] thiadiazole is an azo class constituent unit of a few chemical systems, with a planar geometry contains highly electronegative hetero atoms, a delocalized electron system, and the ability to interact with active second and fifth indispensable positions [27–30, 33, 34]. Triazolo thiadiazole is a critical building block (Fig. 1) for second-order NLO properties, with the ability to improve quadratically second-order NLO properties by selecting the optimal donor–acceptor combination. Numerous research groups have concentrated on triazolo thiadiazole systems, but their efforts have been limited to experimental studies of biological active properties and a few other works on theoretically reported NLO properties [27–30, 33, 34]. No comprehensive theoretical studies of second-order NLO properties have been conducted on the titled chromophores C1–C7 (Fig. 2); thus, this work includes those studies. Systematic computational research of the internal charge transfer mechanism (ICT) and second-order nonlinear optical characteristics of the triazole thiazole bridge as a common acceptor in C1–C7 is conducted. C1–C7 chromophores, as illustrated in Fig. 2, display efficient NLO characteristics

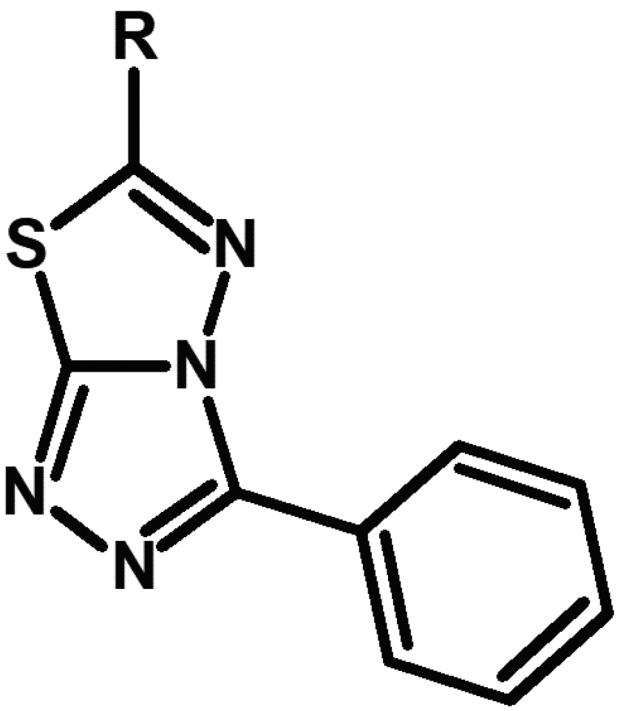

Fig. 1 Building block of triazolo thiadiazole structure

Fig. 2 Chromophores C1–C7

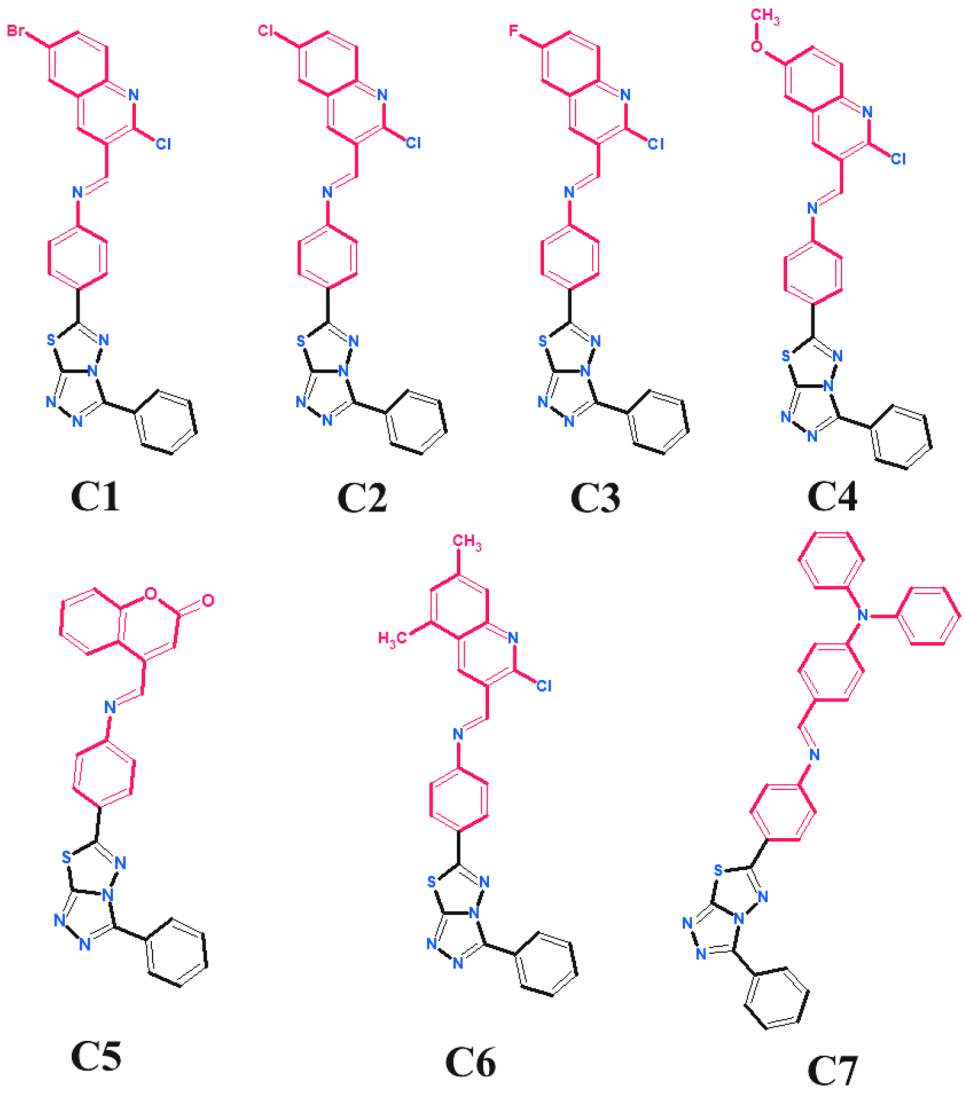

and are persistent. We made use of a time-dependent DFT technique that is not only affordable but also very practicable. Additionally, the influence of donor substitution on second-order NLO properties was investigated using a variety of donor functional groups, including quinoline-substituted halogens, coumarin, methoxy, methyl, and triphenylamine.

Computational methods

All calculations in this work were carried out using the Gaussian 16 program package [37]. Density functional theory (DFT) forms the basis for our measurements. Initially, the structures of molecules C1–C7 were optimized using the Becke Lee Yang and Parr hybrid functional B3LYP/6–311 + + G(d,p) level basis set in C1 symmetry, with global threshold values taken into account in the gaseous phase. The wavefunction stability of each of the optimized structures was verified with the real eigenvalues associated with each structure, and in this case, no negative frequencies were observed. B3LYP has been widely used as a feasible hybrid functional [38–40], but it does not yield qualitative results. To improve accuracy, we used long range corrected (LC) functionals in combination with B3LYP, such as the CAM B3LYP [41] long range corrected with dispersive functional ωB97XD [42]. This combination of LC and B3LYP, along with a triple zeta 6–311 + + G(d,p) level basis set, is most suitable for the entire calculation, and minimizes self-interaction errors. In order to accurately represent the polarization of hydrogen atoms, a d-type basis set was chosen for the fine molecular orbital representation. All other heavy atoms were represented by p-type basis sets. To calculate the molecular nonlinear optical properties of the molecules, such as the dipole moment (μ), polarizability (α), first hyperpolarizability (β), natural bond orbital analysis (NBO), and frontier molecular orbitals (FMO), a time-independent DFT

method was used to calculate the ground state properties. To approximate the vertical energy transitions and to record the UV–visible spectrum accurately, a time-dependent (TD-DFT) method was employed [43].

Results and discussion

Intramolecular charge transfer mechanism

Intramolecular charge transfer (ICT) is an important process in NLO materials. In this process, an electron is transferred from one molecule to another, causing the material to become more electrically polarized, which can lead to a change in the optical properties of the material. This increased polarization can lead to a variety of changes in the material's optical properties, including an increase in its NLO response [44, 45]. In organic molecules, ICT occurs between electron donor (D) and electron acceptor (A) reactive groups of the substituent π conjugated linked to the phenyl rings [44, 45]. Donor building blocks are critical to achieving high NLO response, although acceptor units also play a significant role. In addition, there is a wide range of π-linkers that allows communication between donor and acceptor units. Push–pull architecture is used to design D-π-A organic compounds by incorporating appropriate D, π-bridge, and A units. Increasing asymmetric electronic distribution, reducing charge recombination, inducing charge separation, broadening the absorption range toward longer wavelengths, and decreasing the HOMO–LUMO energy gap all result in an improved NLO response when these push–pull arrangements.

Here in this work [1,2,4] triazolo[3,4-b] [1,3,4] thiadiazole is D-π-A type chromophores (C1–C7) investigated to look into the stabilization, sensitivity, and charge transfer characteristics in order to predict their NLO properties with the help of ICT mechanism. We believed that NLO properties arise due in C1–C7 chromophores (non-centro symmetric) to ICT which involves the transfer of electron density from D toward A units through π-bridge. In this context, subsequent basic parameters (i) dipole moment (μ), (ii) linear polarizability (α), and (iii) first hyperpolarizability (β) were calculated to better understand their NLO properties.

Dipole moment (μ)

The NLO properties primarily set by the molecular dipole moment (μ), which is oriented arbitrarily in a molecular frame. The dipole moment determines the magnitude of the expected NLO coefficient which is greater in the excited state than it is in the ground state due to surrounding influencing media such as solvents, difference in energies

Table 1 Calculated dipole moment (μ) in Debye, polarizability (α) (in 10^{-24} esu), and first hyperpolarizability (β) (in 10^{-34} esu) calculated at B3LYP/6–311 + + G (d, p)

Compound	Dipole moment (μ) in Debye	Polarizability (α) 10^{-24} esu	First hyperpolarizability (β) 10^{-34} esu
C1	2.57	70.86	9852
C2	2.57	69.32	9971.13
C3	2.64	66.58	10,985.9
C4	4.02	70.48	12,975.9
C5	1.54	61.59	30,551.3
C6	3.6	71.73	31,843.9
C7	4.41	86.95	211,167

[46–48]. Equation (1) used to calculate the static dipole moment of C1–C7 in the ground state.

$$\text{Dipole moment}, \mu = \left(\mu_x^2 + \mu_y^2 + \mu_z^2\right)^{\frac{1}{2}} \quad \text{in Debye} \tag{1}$$

The computed values are in the range C5 < C1 ~ C2 < C3 < C4 < C6 < C7 (Tables 1, 2, 3), which suggest that C5 possesses the lowest dipole moment among the molecules. This is because the coumarin-substituted molecule C5 possesses a dipolar structure, and the contribution of free partial charges is low. Appreciable free partial charges in halogens-substituted quinoline molecules C1, C2, and C3 are in increasing order, net dipole moment with respect to decreasing order electronegativity para position-substituted halogens. The molecule of C4 methoxy-substituted quinoline contributes an extremely high amount of partial charges in comparison to the molecule of C6 methyl-substituted quinoline. As a direct result of the existence of oxygen, which causes it to produce an inductively positive impact, C4 is a more polar molecule than C6. Triphenyl amine–substituted C7 molecule is representing the most significant net dipole moment among the all molecules C1–C7, because of its good donating capacity [49].

Table 2 Calculated dipole moment (μ) in Debye, polarizability (α) (in 10^{-24} esu), and first hyperpolarizability (β) (in 10^{-34} esu) calculated at CAM B3LYP/6–311 + + G (d, p)

Compound	Dipole moment (μ) in Debye	Polarizability (α) 10^{-24} esu	First hyperpolarizability (β) 10^{-34} esu
C1	2.57	66.39	11,916.93
C2	2.57	64.96	12,436.23
C3	2.63	62.45	10,098.67
C4	3.98	66.11	21,854.24
C5	1.53	58.16	7570.67
C6	3.56	67.28	32,801.62
C7	4.21	80.48	118,597.15

Table 3 Calculated dipole moment (μ) in Debye, polarizability (α) (in 10^{-24} esu), and first hyperpolarizability (β) (in 10^{-34} esu) calculated at ωB97XD/6–311 + + G (d, p)

Compound	Dipole moment (μ) in Debye	Polarizability (α) 10^{-24} esu	First hyperpolarizability (β) 10^{-34} esu
C1	2.58	66.18	12,748.26
C2	2.57	64.73	13,278.65
C3	2.65	66.22	11,648.35
C4	3.98	65.88	21,688.49
C5	1.55	50.02	5904.88
C6	3.55	67.03	30,898.83
C7	4.19	80.00	105,032.98

Linear polarizability (α)

The optical response consistency is defined by the materials electrical properties, namely linear polarizability (α), which is a measurable physical molecular property, describes the induced dipole moment in the direction of applied external field, and always tied to the structure, bonding effects, and net dipole moment of the materials system. Linear polarizability of output values are (Tables 1, 2, 3) estimated with Eq. (2).

$$\alpha = \left(\frac{1}{3}\right)\left[\alpha_{xx} + \alpha_{yy} + \alpha_{zz}\right] \quad \text{in esu} \tag{2}$$

The computed values of C1–C7 are found in increasing order (Tables 1, 2, 3) of the net dipole moment, directly proportional to the number of charges and size of the atom. Amid quinoline-substituted molecules are found in increasing order due to polarity of the molecules substituted with halogens in size and contribution of partial charges; similarly, triphenyl amine is more in donating charges than methoxy- and methyl-substituted group molecules.

First hyperpolarizability

First hyperpolarizability (β) is principal key factor for describing strength of second-order NLO materials [50]. It is third rank tensor, highly structure oriented in π-conjugated push–pull path molecular systems. Total β of chromophores C1–C7 is estimated at frequency-dependent applied field, energy as a function of derivatives in theoretical frame using Eq. (3).

$$\beta_{total} = \left[\left(\beta_{xxx} + \beta_{xyy} + \beta_{xzz}\right)^2 + \left(\beta_{yyy} + \beta_{xxy} + \beta_{yyz}\right)^2 + \left(\beta_{zzz} + \beta_{xxz} + \beta_{yyz}\right)^2\right]^{\frac{1}{2}} \tag{3}$$

Structurally, C1–C7 are non-centro symmetric in nature and values of total β are found in order of C1 < C2 < C3 < C4 < C5 < C6 < C7 (Tables 1, 2, 3), C = N imine linkage acts as a π acceptor, connected at one end and acceptor triazolo thiadiazole ring at another end. In C1–C4, halogens-substituted quinoline molecules, halogens show a dual nature, both donor and acceptor. The presence of electron deficient nitrogen in quinoline and high electronegative halogens act as donor rather than acceptor, but the collective effect is donating. Therefore, the contribution of charges is poor; first, hyperpolarizability is low and increased within as electronegativity decreases in C1–C4. C6 has a higher β value than C4, because of delocalization of electrons and donating capacity of charge is more in methyl group than methoxy. Magnitude of first hyperpolarizability is increased in C5 coumarin-substituted molecules even though has low dipole moment, due to presence of oxygen, which indicates it is a good donor. Delocalization of π electrons is more in triphenyl amine–substituted molecule C7 exhibiting larger value lone pair delocalization and it has best donating capacity of electrons.

Frontier molecular orbitals

The highest occupied molecular orbitals (HOMO) and lowest unoccupied molecular orbitals (LUMO) are in conjunction termed as frontier molecular orbitals (FMO), which signifies chemical reactivity and kinetic stability of the molecular systems [51, 52]. It provides the information of energetic behavior and the ability to withdraw and donate an electron in addition to the electron transport properties, dynamic stability, chemical hardness, chemical reactivity, and softness of the molecules. The larger the HOMO–LUMO gap ($E_{gap} = E_{LUMO} - E_{HOMO}$) signifies hard nature of the molecule, the smaller the gap soft and more reactive and stable [53].

Figure 3 shows the FMO for π → π* interactions calculated at B3LYP/6–311 + + G (d, p) [with iso surface value is − 10e to 10e]. The negative charge phase (red color) and positive charge phase (green color) patterns in Fig. 3 approximated throughout the molecule using optimized structure C1–C7. Values of C1–C7 follow a similar trend, in the interval of 0.11–0.13 eV in (Table 4), a narrow energy gap between observed due to stronger donating capacity in triphenyl substituted molecules with strong acceptor and weak donor. Strong acceptor in the rest of the molecules listed in Table 4. Molecules HOMO orbital localized over triazolo thiadiazole moiety and LUMO orbitals extended over the substituted donor overlapped each other.

Chemical hardness is connected with HOMO–LUMO; it is a measure of a molecule's resistant to charge movement and it is related to longevity and sensitivity [54, 55]. It can be computed using Eq. (4)

$$\eta = \frac{1}{2}\left[E_{LUMO} - E_{HOMO}\right] \tag{4}$$

Similarly, chemical softness is defined as the ability to draw electron flow. It is tied to a polarizability characteristic and can be determined utilizing Eq. (5)

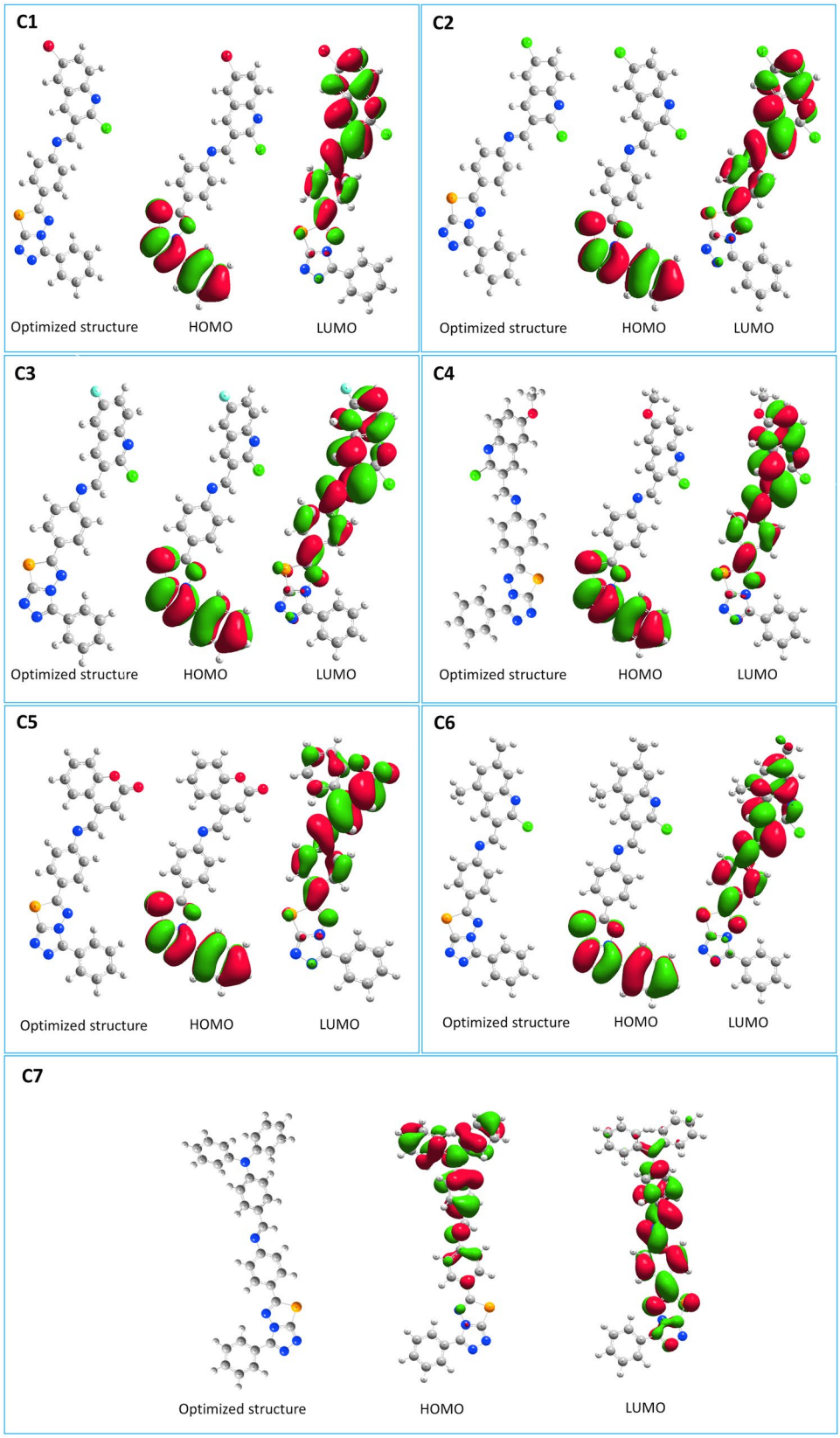

Fig. 3 Frontier molecular orbitals for $\pi \rightarrow \pi^*$ interactions calculated at B3LYP/6–311 + + G (d, p)

Table 4 Chemical hardness (η) (in au^{-1}), chemical softness (σ) (in au^{-1}), HOMO and LUMO (in eV) for $\pi \rightarrow \pi^*$ interactions calculated at B3LYP/6–311 + + G (d, p)

Molecule	Chemical hardness	Chemical softness	HOMO	LUMO	Energy gap (eV)
C1	0.06	16.67	−0.23	−0.11	0.12
C2	0.06	16.67	−0.23	−0.11	0.12
C3	0.06	16.67	−0.23	−0.11	0.12
C4	0.06	16.67	−0.23	−0.11	0.12
C4	0.05	20	−0.23	−0.11	0.12
C6	0.065	16.67	−0.23	−0.10	0.13
C7	0.055	20	−0.20	−0.09	0.11

$$\sigma = \frac{1}{\eta} \tag{5}$$

The chromophores C1–C7 listed the values of chemical softness and chemical hardness, also from HOMO–LUMO band gap is very narrow; hence, they are soft in nature and chemically reactive, aromatic, and polarizable. The low band-gap energy of these conjugated chromophores makes them particularly suitable for prospective optoelectronic applications.

Natural bond orbitals

The natural bond orbital (NBO) analysis is a method that is used to examine the molecular orbitals of a molecule. This analysis can be used to determine the stability of a molecule and to identify possible electron donors and acceptors. The NBO analysis can also be used to determine electronic structure of molecules. In this analysis, the orbitals of the molecule are divided into two categories: bonding and antibonding. The bonding orbitals are those that contribute to the formation of chemical bonds, while the antibonding orbitals are those that oppose the formation of chemical bonds. Moreover, it is estimated the redistribution of electron density in different bonding and antibonding situations. Second-order perturbation energy mechanism is often applying to study the interaction between donor and corresponding acceptor through NBO [56, 57]. It helps to evaluate the stability of chemical bonding and the transfer of charge in the molecule. It assessed with Eq. (6).

$$\text{The quantities of } E \qquad E^{(2)} = q_i \frac{F^2(i,j)}{\varepsilon_j - \varepsilon_i} \tag{6}$$

where $F^2(i,j)$ represents the off-diagonal matrix elements, q_i gives the donor orbital's occupancy, ε_j and ε_i provide the values of donor and acceptor orbital energies. $E^{(2)}$ estimates the magnitude of interaction between the donor and acceptor orbitals; it also demonstrates delocalization across chemical species. Here we have listed (Table 5) some exceptional interactions between bonding or lone pair. Lewis type NBO occupied orbitals contrasted with non-Lewis type NBO unoccupied orbitals of molecules. In C1–C7 molecules $n \rightarrow \pi$ and $\pi \rightarrow \pi^*$ (Table 5) which indicate contribution of charge from lone pair of electrons to adjacent π bond and π bond to corresponding conjugated π bond signify the interactions between different donors and acceptors across chemical species.

Table 5 Some selected most effective second-order perturbation (E^2) interactions are listed for evaluation of hyperconjugation energies (kcal/mol) calculated at B3LYP/6–311 + + G(d, p)

Interactions	C1	C2	C3	C4	C5	C6	C7
n_{Br33}-$\pi_{C30–C31}$	1.85	-	-	-	-	-	-
n_{Cl33}-$\pi_{C30–C31}$	-	1.95	-	-	-	-	-
n_{F33}-$\pi_{C29–C30}$	-	-	4.35	-	-	-	-
n_{O33}-$\pi_{C30–C31}$	-	-	-	12.03	-	-	-
n_{O33}-$\pi_{C25–C27}$	-	-	-	-	2.88	-	-
n_{N21}-$\pi_{C1–C3}$	-	-	-	-	-	5.51	-
$\pi_{C31–C35}$-$\pi_{C27–C32}$	-	-	-	-	-	53.39	-
$\pi_{C31–C35}$-$\pi_{C27–C32}$	-	-	-	-	-	2.83	-
n_{N1}-$\pi_{C14–C16}$	-	-	-	-	-	-	29.73
$\pi_{C14–C16}$-$\pi_{C15–C17}$	-	-	-	-	-	-	231.01
$\pi_{C27–O28}$-$\pi_{C23–C25}$	-	-	-	-	13	-	-
$\pi_{C26–N28}$-$\pi^*_{C23–C24}$	9.55	9.62	1.40	16.80	-	9.26	-
$\pi_{C29–C30}$-$\pi^*_{C25–C27}$	23.06	18.21	5.63	22.31	-	14.56	-
$\pi_{N21–C22}$-$\pi^*_{C1–C3}$	1.13	1.14	1.15	1.22	1.67	9.92	10.64
$\pi_{C1–C3}$-$\pi^*_{C5–C6}$	23.78	23.78	2084	22.82	-	26.65	-
$\pi_{C5–C6}$-$\pi^*_{C7–N8}$	20.80	20.82	22.08	22.80	-	21.45	-
$\pi_{C12–N13}$-$\pi^*_{C15–C16}$	7.06	7.08	5.08	8.63	25.76	81.10	16.28
Total charge	87.23	82.6	60.53	83.07	73.04	225.38	287.66

Molecular electrostatic potential (MEP)

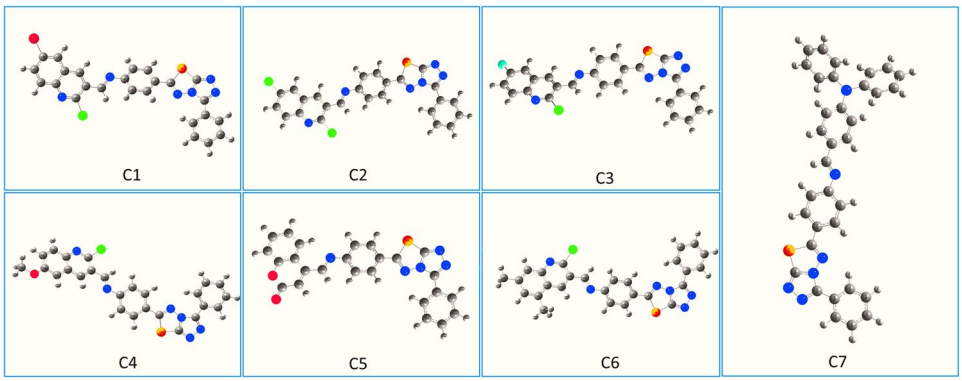

Fig. 4 Schematic charge in flow in molecule C1–C7

The most efficient charge transfer occurs in $\pi_{C14–C16}$-$\pi_{C15–C17}$. Charge flow from donor triphenyl ring to acceptor triazolo thiadiazole through phenyl ring with avail value 231 kcal/mole in chromophore C7. Similarly, $\pi_{C31–C35}$-$\pi_{C27–C32}$ reflects interactions C6 values 53.90 kcal/mole, as $\pi \rightarrow \pi^*$ interactions followed a similar path in C1, C2, C3, and C4 molecules (Fig. 4). Charge transfer of C1–C7 values is in the sequence of C3 < C5 < C2 < C4 < C1 < C6 < C7. Halogens enclosed moieties least in charge of overall charge transfer due to their dual nature they behave as acceptor instead of donor indicates lower hyperpolarizability. Triphenylamine has massive charge transfer, indicates a higher degree of hyperpolarizability which is superior to other molecules such as C4, C5, and C6 in terms of hyperpolarizability value. It has a high electron-donating ability due to their extended conjugation and delocalization charges and nitrogen lone pair effect. C6 is higher than halogen-substituted molecules due to their extended conjugation with a combination of the substantial donor C1, C2, C3, and C4 have relatively lower than C6 due to presence of halogens.

A molecular electrostatic potential is a valuable method for analyzing reactive nature and assessing electron density. It illustrates the concept of electrophilic and nucleophilic reactive cites in intramolecular interactions [58]. MEP surface C1–C7, the surface and curve, are shown in Fig. 5 and Fig. 6 and it is obtained using a B3LYP/6–311 + + G (d, p) level basis set for optimised geometry. The electrostatic potential surface of C1–C7 is shown in Fig. 5. The negative regions (red, yellow, and green) show electrophilic reactivity, while the positive regions (blue) are showing nucleophilic reactivity (Fig. 5). C1–C7 chromophore structures are similar except for the donor part (Fig. 5). The electron density is higher in the acceptor triazole thiadiazole region, where the N = N bond exists, and lower in the donor triazole thiadiazole area, where the C-H bond exists. This demonstrates that the donating (blue) part of C1–C7 is nucleophilic and implies more

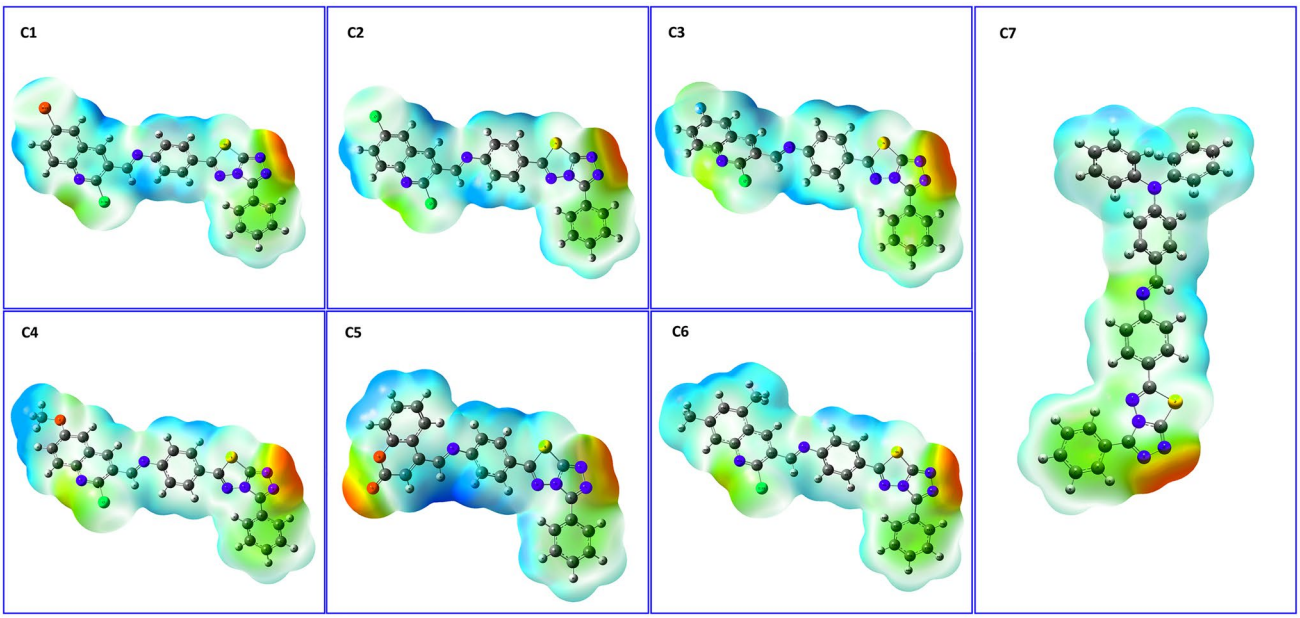

Fig. 5 Electrostatic potential surface C1–C7

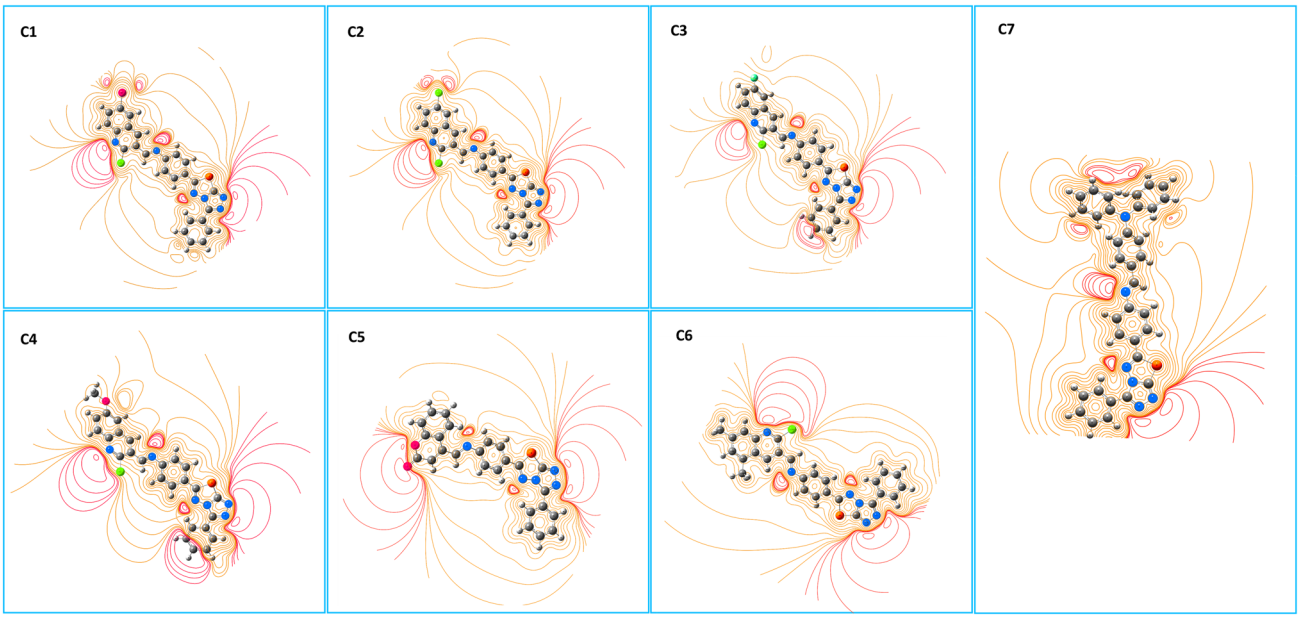

Fig. 6 Electrostatic potential curves C1–C7

chances of intramolecular interactions at N = N, C-H bond connecting regions. Additionally, the O = C region of C5 coumarin-substituted molecules is a denser acceptor region and can interact next to adjacent C-H bonds. The C1–C7 MEP curve shows a C-H bond expanded potential positive curve (Fig. 6) toward a negative region N = N; at this point, the possibility of intramolecular interactions can occur.

UV–Vis spectra

The UV–visible spectrum is crucial in understanding the optical properties of a conjugated chemical species. The spectrum recorded using TD-DFT B3LYP/6–311 + + G (d, p) level basis set, with both the wavelength and oscillator strength of C1–C7 listed in Table 6 [43]. It is shown in Table 6 how the different donors' groups in its substitution have an effect on the first π-π* electronic transitions in the sequence of molecules. A bathochromic transition shift is observed from C1 to C7, and followed as C4 < C6 < C5 < C3 < C2 < C1 < C7. The strength of the corresponding oscillator illustrates that HOMO–LUMO transitions dominate significant changes in the intensities of these electronic transitions. Elevated wavelength absorbed as a consequence of enhanced conjugated structure in the donor part of C7, visible for the π-π* character.

Figure 7 shows the UV–Vis spectrum recorded at B3LYP/6–311 + + G (d, p) with 30 number of excited states. The wavelength of absorbance throughout the violet and blue color region of the spectrum extends (Fig. 7). Because of the presence of strong donors and strong acceptors in C7, bathochromic shift in C7 occurs in the visible spectrum region, whereas strong acceptors are present in the remaining of the molecules (C1–C6), resulting in bathochromic shift in the ultraviolet spectrum region.

The transitions of C1–C7 chromophores are primarily derived from the HOMO → LUMO transition, which is consistent with the laws of most D-π-A organic compounds in their structure. It is noteworthy from the prior discussion that the decreasing order of β is consistent with the decreasing order of average polarizability, which is further consistent with the growing order of the HOMO–LUMO energy gap, as previously discussed. Furthermore, it is evident and widely known that the larger HOMO–LUMO gap of C6 chromophore exhibits weak NLO response, whereas the lower HOMO–LUMO gap of C7 chromophore exhibits the maximum NLO response, as previously stated. In light of the preceding discussion, it is clear that managing the type of π-bridges and acceptor units is an essential method for the development of visually appealing NLO materials. According to our expectations, this new

Table 6 UV–Vis spectrum, oscillator strength recorded at B3LYP/6–311 + + G (d, p) with $n = 30$ (number of states) wavelength (nm)

Compound	C1	C2	C3	C4	C5	C6	C7
Wavelength	397.74	397.47	395.81	389.64	394.47	393.17	435.53
Oscillator strength	0.7750	0.7621	0.7457	0.8398	0.4934	0.9735	1.1037

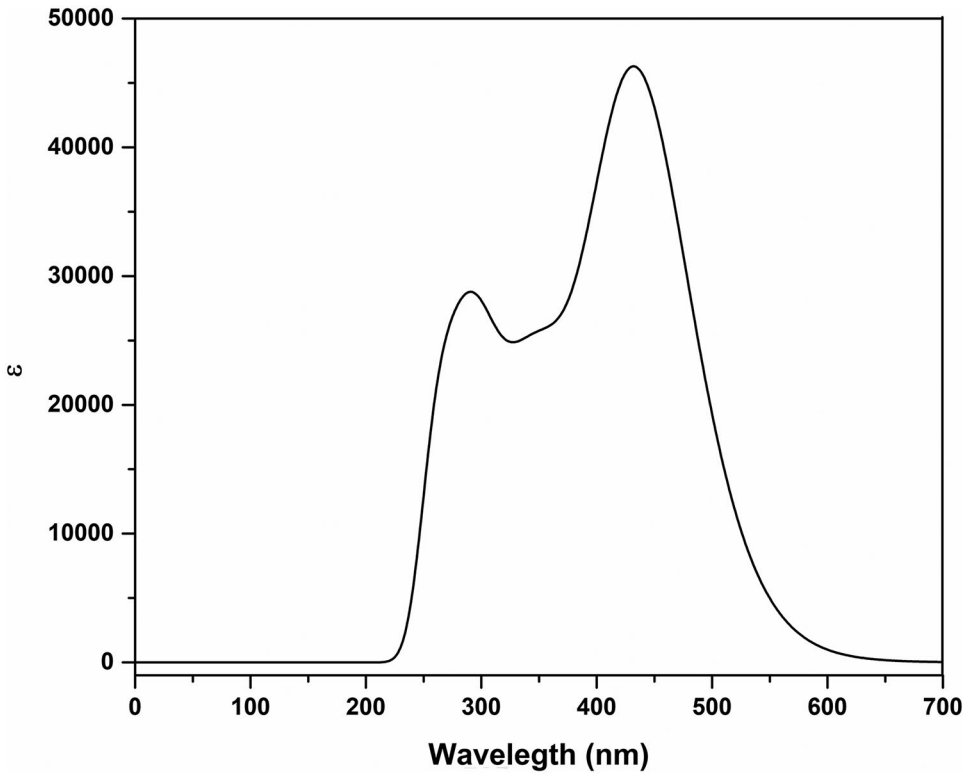

Fig. 7 UV–Vis spectrum recorded at B3LYP/6–311 + + G (d, p) with $n = 30$ (n is number of excited states; and wavelength in nm)

understanding of the effects of π-bridges and acceptor units on NLO properties will be utilized to the construction of innovative NLO materials with optical and photoelectric tools are excellent performance in modern advanced applications.

Conclusions

Nonlinear optical (NLO) materials are of great interest in photon-based communication, sensing, and biomedical applications. These plasmonic compounds are typically designed to achieve a desired NLO property. Optimized geometry and stability of structures of C1–C7 molecules are checked at ground state, and studied their second-order NLO properties with DFT and TD-DFT method. NLO active triazolo thiadiazole chromophores substitutional impact on second-order NLO coefficients extensively by different donor groups. Methoxy methyl and triphenylamine donor substitution molecules show massive charge transfer and first hyperpolarizability values $21{,}688.49 \times 10^{-34}$ esu, $30{,}898.83 \times 10^{-34}$ esu, and $105{,}032.98 \times 10^{-34}$ esu respectively. The HOMO and LUMO energy levels of chromophores indicate that electron transfer can take place with low bandgap molecules, making them more stable and chemically reactive. This makes them suitable for photophysical and optoelectronic applications. Furthermore, intramolecular interactions induce a redshift in the UV–visible spectrum due to the strong donor triphenylamine in C7, which enhances the nonlinear optical (NLO) response. These findings suggest that the choice of donor and acceptor can have a significant effect on the first hyperpolarizability, making these chromophores promising NLO materials for Second Harmonic Generation-based Photonic devices, such as memory devices. Theoretical calculations and approximations were carried out in the gas phase using the hybrid functionals, with the most suitable method being ωB97XD for NLO property calculations. These results encourage further experimental studies.

Acknowledgements The authors gratefully thank the Chairman, Department of PG studies in Chemistry and Coordinator of Molecular Modelling Lab under UPE FAR-I & DST PURSE Phase-II Programme at Karnatak University Dharwad, for providing the computational facility to the present work.

Author contribution The conceptualization and design of the study were collective efforts from all of the authors. Mr. Balachandar Waddar was responsible for the material simulations, data gathering, and analysis, while Dr. Saidi Reddy Parne was responsible for the conceptualization, reviewing and editing, resources, and supervision of the project. Dr. Suman Gandi, Dr. Gurusiddappa R. Prasanth, Mr. Mohammed Yaseen, and Dr. Mahadevappa Y. Kariduraganavar were responsible for the reviewing and editing, as well as the resources and formal analysis. Previous versions of the paper were discussed and commented on by all of the authors. The final text was reviewed and approved by all of the authors.

Availability of data and materials All data are available on request to the corresponding author.

Code availability Not applicable.

Declarations

Ethical approval Not applicable.

Conflict of interest The authors declare no competing interests.

References

1. Marder SR, Perry JW (1993) Molecular materials for second-order nonlinear optical applications. Adv Mater 5:804–815. https://doi.org/10.1002/adma.19930051104
2. Abdullah M, Bakhtiar H, Krishnan G, Aziz M, Danial W, Islam S (2019) Transition from saturable absorption to reverse saturable absorption of carmoisine dye under low-powered continuous wave laser excitation. Opt Laser Technol 115:97–103. https://doi.org/10.1016/j.optlastec.2019.01.032
3. Bredas JL, Adant C, Tackx P, Persoons A, Pierce B (1994) Third-order nonlinear optical response in organic materials: theoretical and experimental aspects. Chem Rev 94:243–278. https://doi.org/10.1021/cr00025a008
4. Notake T, Takeda M, Okada S, Hosobata T, Yamagata Y, Minamide H (2019) Characterization of all second-order nonlinear-optical coefficients of organic N-benzyl-2-methyl-4-nitroaniline crystal. Sci Rep 9:1–8. https://doi.org/10.1038/s41598-019-50951-1
5. Najare MS, Patil MK, Garbhagudi M, Yaseen M, Inamdar SR, Khazi IAM (2021) Design, synthesis and characterization of π-conjugated 2, 5-diphenylsubstituted-1, 3, 4-oxadiazole-based D-π-A-π'-D′ form of efficient deep blue functional materials: Photophysical properties and fluorescence "Turn-off" chemsensors approach. J Mol Liq 328:11544. https://doi.org/10.1016/j.molliq.2021.115443
6. Ullah F, Deng N, Qiu F (2021) Recent progress in electro-optic polymer for ultra-fast communication. PhotoniX 2:13. https://doi.org/10.1186/s43074-021-00036-y
7. Abudurusuli A, Li J, Pan S (2021) A review on the recently developed promising infrared nonlinear optical materials. Dalton Trans 50:3155–3160. https://doi.org/10.1039/d1dt00054c
8. Tsutsumi N, Morishima M, Sakai W (1998) Nonlinear optical (NLO) polymers. 3. NLO polyimide with dipole moments aligned transverse to the imide linkage. Macromolecules 31:7764–7769. https://doi.org/10.1021/ma9803436
9. Breitung EM, Shu C-F, McMahon RJ (2000) Thiazole and thiophene analogues of donor− acceptor stilbenes: molecular hyperpolarizabilities and structure− property relationships. J Am Chem Soc 122:1154–1160. https://doi.org/10.1021/ja9930364
10. Colombo A, Dragonetti C, Guerchais V, Hierlinger C, Zysman-Colman E, Roberto D (2020) A trip in the nonlinear optical properties of iridium complexes. Coord Chem Rev
11. Prasad PN (1989) Nonlinear optical effects in organic molecules and polymers-theory, measurements and devices. In Optical Materials Technology for Energy Efficiency and Solar Energy Conversion. Proc SPIE Int Soc Opt Photonics 1016:2–11. https://doi.org/10.1117/12.949907
12. Dalton LR, Sullivan PA, Bale DH (2010) Electric field poled organic electro-optic materials: state of the art and future prospects. Chem Rev 110:25–55. https://doi.org/10.1021/cr9000429
13. Luo X, Li Z, Guo Y, Yao J, Wu Y (2019) Recent progress on new infrared nonlinear optical materials with application prospect. J Solid State Chem 270:674–687. https://doi.org/10.1016/j.jssc.2018.12.036
14. You J, Bongu S, Bao Q, Panoiu N (2019) Nonlinear optical properties and applications of 2D materials: theoretical and experimental aspects. Nanophotonics 8:63–97. https://doi.org/10.1515/nanoph-2018-0106
15. Karna SP (2000) Electronic and nonlinear optical materials: the role of theory and modeling. J Phys Chem A 104:4671–4673. https://doi.org/10.1021/jp001296y
16. Bhattacharya S, Biswas C, Raavi SS, Venkata Suman Krishna J, Vamsi Krishna N, Giribabu L, Soma VR (2019) Synthesis, optical, electrochemical, DFT studies, NLO properties, and ultrafast excited state dynamics of carbazole-induced phthalocyanine derivatives. J Phys Chem C 123:11118–11133. https://doi.org/10.1021/acs.jpcc.9b01531
17. Akram M, Adeel M, Khalid M, Tahir MN, Khan MU, Asghar MA, Ullah MA, Iqbal M (2018) A combined experimental and computational study of 3-bromo-5-(2, 5-difluorophenyl) pyridine and 3, 5-bis (naphthalen-1-yl) pyridine: insight into the synthesis, spectroscopic, single crystal XRD, electronic, nonlinear optical and biological properties. J Mol Struct 1160:129–141. https://doi.org/10.1016/j.molstruc.2018.01.100
18. Ahmad MS, Khalid M, Shaheen MA, Tahir MN, Khan MU, Braga AA, Shad HA (2018) Synthesis and XRD, FT-IR vibrational, UV–vis, and nonlinear optical exploration of novel tetra substituted imidazole derivatives: a synergistic experimental-computational analysis. J Phys Chem Solids 115:265–276. https://doi.org/10.1016/j.jpcs.2017.12.054
19. Shen Y, Tang W, Lin X (2022) Advances in second-order nonlinear optical sulfates. Coord Chem Rev 459:214443. https://doi.org/10.1016/j.ccr.2022.214443
20. Wu J, Luo J, Jen AK-Y (2020) High-performance organic second- and third-order nonlinear optical materials for ultrafast information processing. J Mat Chem C 8:15009–15026. https://doi.org/10.1039/D0TC03224G
21. Yahya M, Nural Y, Seferoğlu Z (2022) Recent advances in the nonlinear optical (NLO) properties of phthalocyanines: a review. Dyes and Pigm 198:109960. https://doi.org/10.1016/j.dyepig.2021.109960
22. Bosshard C, Sutter K, Prêtre P, Hulliger J, Flörsheimer M, Kaatz P, Günter P (1995) Organic nonlinear optical materials. CRC Press, London. https://doi.org/10.1201/9780429114090
23. Suresh S, Ramanand A, Jayaraman D, Mani P (2012) Review on theoretical aspect of nonlinear optics. Rev Adv Mater Sci 30:175–183
24. Marder SR (2006) Organic nonlinear optical materials: where we have been and where we are going. Chem Commun 131–134. https://doi.org/10.1039/B512646K
25. Laurent AD, Adamo C, Jacquemin D (2014) Dye chemistry with time-dependent density functional theory. Phys Chem Chem Phys 16:14334–14356. https://doi.org/10.1039/C3CP55336A
26. Laurent AD, Jacquemin D (2013) TD-DFT benchmarks: a review. Int J Quantum Chem 113:2019–2039. https://doi.org/10.1002/qua.24438
27. Wu S, Shi J, Chen J, Hu D, Zang L, Song B (2021) Synthesis, antibacterial activity, and mechanisms of novel 6-sulfonyl-1, 2, 4-triazolo [3, 4-b][1, 3, 4] thiadiazole derivatives. J Agric Food Chem 69:4645–4654. https://doi.org/10.1021/acs.jafc.1c01204
28. Radwan AA, Alanazi FK, Al-Agamy MH (2017) 1, 3, 4-Thiadiazole and 1, 2, 4-triazole-3 (4H)-thione bearing salicylate moiety: synthesis and evaluation as anti-Candida albicans. Braz J Pharm Sci 53:e15239. https://doi.org/10.1590/s2175-97902017000115239
29. Lin L, Liu H, Wang DJ, Hu YJ, Wei XH (2017) Synthesis and biological activities of 3, 6-disubstituted-1, 2, 4-triazolo-1, 3, 4-thiadiazole derivatives. Bull Chem Soc of Ethiop 31:481–489. https://doi.org/10.4314/bcse.v31i3.12
30. Pandey AK, Shukla DV, Singh V, Narayan V (2018) Structural, IR spectra NBO, TDDFT, AIM calculation, biological activity and docking property of [1, 2, 4]-triazolo [3, 4-b][1, 3, 4] thiadiazole. Egypt J Basic Appl Sci 5:280–288. https://doi.org/10.1016/j.ejbas.2018.10.001

31. Gao F, Wang T, Xiao J, Huang G (2019) Antibacterial activity study of 1, 2, 4-triazole derivatives. Eur J Med Chem 173:274–281. https://doi.org/10.1016/j.ejmech.2019.04.043
32. Shamroukh AH, Hegab MI (2020) A review on synthesis, therapeutic, and computational studies of substituted 1, 3, 4 thiadiazole derivatives. Egyp J Chem 63:4387–4408. https://doi.org/10.21608/ejchem.2020.25343.2492
33. Bhat KS, Prasad DJ, Poojary B, Holla BS (2004) Synthesis of some new 1, 2, 4-triazolo [3, 4-b]-thiadiazole derivatives as possible anticancer agents. Phosphorus Sulfur Silicon Relat Elem 179:1595–1603. https://doi.org/10.1080/10426500490464186
34. Fusco S, Centore R, Riccio P, Quatela A, Stracci G, Archetti G, Kuball H-G (2008) NLO-active polymers containing triazolo-thiadiazole segments. Polymer 49:186–191. https://doi.org/10.1016/j.polymer.2007.11.016
35. Capobianco A, Centore R, Fusco S, Peluso A (2013) Electro-optical properties from CC2 Calculations: a comparison between theoretical and experimental results. Chem Phys Lett 580:126–129. https://doi.org/10.1016/j.cplett.2013.07.004
36. Doddamani RV, Rachipudi PS, Inamdar SR, Kariduraganavar MY (2019) Enhancement of nonlinear optical and thermal properties of polyurethanes by modifying the chromophores with fused heterocyclic and pyrimidine rings. Polym Eng Sci 59:500–509. https://doi.org/10.1002/pen.24957
37. Me F, Trucks G, Schlegel H, Scuseria G, Robb M, Cheeseman J, Scalmani G, Barone V, Petersson G, Nakatsuji H (2016) Gaussian 16. Gaussian, Inc., Wallingford, CT
38. Zhang IY, Wu J, Xu X (2010) Extending the reliability and applicability of B3LYP. Chem Commun 46:3057–3070. https://doi.org/10.1039/C000677G
39. Dreuw A, Head-Gordon M (2005) Single-reference ab initio methods for the calculation of excited states of large molecules. Chem Rev 105:4009–4037. https://doi.org/10.1021/cr0505627
40. Parr RG, Szentpály LV, Liu S (1999) Electrophilicity index. J Am Chem Soc 121:1922–1924. https://doi.org/10.1021/ja983494x
41. Mehboob MY, Hussain R, Adnan M, Farwa U, Irshad Z, Janjua MR (2021) Theoretical modelling of novel indandione-based donor molecules for organic solar cell applications. J Phy Chem Solids 162:110508. https://doi.org/10.1016/j.jpcs.2021.110508
42. Chai JD, Head-Gordon M (2008) Long-range corrected hybrid density functionals with damped atom–atom dispersion corrections. Phys Chem Chem Phy 10:6615–6620. https://doi.org/10.1039/B810189B
43. Pandey N, Mehata MS, Pant S, Tewari N (2021) Structural, electronic and NLO properties of 6-aminoquinoline: a DFT/TD-DFT study. J Fluoresc 31:1719–1729. https://doi.org/10.1007/s10895-021-02788-z
44. Oudar JD (1977) Optical nonlinearities of conjugated molecules. Stilbene derivatives and highly polar aromatic compounds. J Chem Phys 67:446–457. https://doi.org/10.1063/1.434888
45. Zyss J (1979) Hyperpolarizabilities of substituted conjugated molecules. II. Substituent effects and respective σ–π contributions. J Chem Phys 70:3341–3349. https://doi.org/10.1063/1.437919
46. Oudar JL, Chemla DS (1977) Hyperpolarizabilities of the nitroanilines and their relations to the excited state dipole moment. J Chem Phys 66:2664–2668. https://doi.org/10.1063/1.434213
47. Jiang X, Zhao S, Lin Z, Luo J, Bristowe PD, Guan X, Chen C (2014) The role of dipole moment in determining the nonlinear optical behavior of materials: ab initio studies on quaternary molybdenum tellurite crystals. J Mater Chem C 2:530–537. https://doi.org/10.1039/C3TC31872A
48. Yanagi K, Kobayashi T, Hashimoto H (2003) Origin of transition dipole-moment polarizability and hyperpolarizability in hydrazones. Phys Rev B 67:115122. https://doi.org/10.1103/PhysRevB.67.115122
49. Zhang T, Brumboiu IE, Grazioli C, Guarnaccio A, Coreno M, de Simone M, Santagata A, Rensmo H, Brena B, Lanzilotto V, Puglia C (2018) Lone-Pair delocalization effects within electron donor molecules: the case of triphenylamine and its thiophene-analog. J Phys Chem C 122:17706–17717. https://doi.org/10.1021/acs.jpcc.8b06475
50. Parthasarathy V, Pandey R, Das PK, Castet F, Blanchard-Desce M (2018) Linear and nonlinear optical properties of tricyanopropylidene-based merocyanine dyes: synergistic experimental and theoretical investigations. ChemPhysChem 19:187–197. https://doi.org/10.1002/cphc.201701143
51. Drissi M, Benhalima N, Megrouss Y, Rachida R, Chouaih A, Hamzaoui F (2015) Theoretical and experimental electrostatic potential around the m-nitrophenol molecule. Molecules 20:4042–4054. https://doi.org/10.3390/molecules20034042
52. Sebastian S, Sundaraganesan N (2010) The spectroscopic (FT-IR, FT-IR gas phase, FT-Raman and UV) and NBO analysis of 4-Hydroxypiperidine by density functional method. Spectrochim Acta Part A Mol Biomol Spectrosc 75:941–952. https://doi.org/10.1016/j.saa.2009.11.030
53. Xavier S, Periandy S, Ramalingam S (2015) NBO, conformational, NLO, HOMO–LUMO, NMR and electronic spectral study on 1-phenyl-1-propanol by quantum computational methods. Spectrochim Acta Part A Mol Biomol Spectrosc 137:306–320. https://doi.org/10.1016/j.saa.2014.08.039
54. Zarate X, Schott E, Gomez T, Arratia-Pérez R (2013) Theoretical study of sensitizer candidates for dye-sensitized solar cells: peripheral substituted dizinc pyrazinoporphyrazine–phthalocyanine complexes. J Phys Chem A 117:430–438. https://doi.org/10.1021/jp3067316
55. Srivastava A, Rawat P, Tandon P, Singh RN (2012) A computational study on conformational geometries, chemical reactivity and inhibitor property of an alkaloid bicuculline with γ-aminobutyric acid (GABA) by DFT. Comput Theor Chem 993:80–89. https://doi.org/10.1016/j.comptc.2012.05.025
56. Landis CR, Cleveland T, Firman TK (1998) Valence bond concepts applied to the molecular mechanics description of molecular shapes. 3. Applications to transition metal alkyls and hydrides. J Am Chem Soc 120:2641–2649. https://doi.org/10.1021/ja9734859
57. Reed AE, Weinstock RB, Weinhold F (1985) Natural population analysis. J Chem Phys 83:735–746. https://doi.org/10.1063/1.449486
58. Ayare NN, Rajeshirke M, Sreenath MC, Chitrambalam S, Joe IH, Sekar N (2019) NLO-phoric emissive quinoxaline analog of Quinoline Yellow 54 and Z-Scan studies. ChemistrySelect 4:3752–3761. https://doi.org/10.1002/slct.201900040